Optical methods and sensor development for cellular level imaging

Nihal Muhammed Habeeb

MS15010

A dissertation presented for the partial fulfilment of BS-MS Dual Degree in Science

Indian Institute of Science Education and Research, Mohali

June 2020

Dedicated to:

My Family and Friends

Certificate of Examination

This is to certify that the dissertation titled "**Optical methods and sensor development for cellular level imaging**" submitted by **Mr. Nihal Muhammed Habeeb** (Reg. No. MS15010) for the partial fulfilment of BS-MS dual degree programme of Indian Institute of Science Education and Research, Mohali has been examined by the thesis committee duly appointed by the institute. The committee finds the work done by the candidate satisfactory and recommends that the report be accepted.

Dr. Samir Kumar Biswas (Supervisor)

Dr. Sandeep K Goyal

Dr. Vishal Bhardwaj

Dated: June 11, 2020

Declaration

The work presented in this dissertation has been carried out by me under the guidance of Dr. Samir Kumar Biswas at the Indian Institute of Science Education and Research, Mohali.

This work has not been submitted in part or in full for a degree, a diploma, or a fellowship to any university or institute. Whenever contributions of others are involved, every effort is made to indicate this clearly, with due acknowledgement of collaborative research and discussion. This thesis is a bonafide record of original work done by me and all sources listed within have been detailed in the bibliography.

Nihal Muhammed Habeeb

(Candidate)

Dated: June 11, 2020

In my capacity as the supervisor of the candidate's project work, I certify that the above statements by the candidate are true to the best of my knowledge.

Dr. Samir Kumar Biswas

(Supervisor)

Acknowledgment

Firstly, I would like to express my gratitude to Dr. Samir Kumar Biswas for his mentorship throughout this project, the constructive comments and the independence he gave me to execute my research. Without his guidance, this dissertation would not have been possible.

I would like to thank Dr. Sandeep K Goyal and Dr. Vishal Bhardwaj, the members of my thesis committee for the discussions during the presentations which helped me shape my work further.

I would like to thank my colleagues in the Bio Nano Photonics lab, Dr. Sriram Krishnan, Sumith K K, Asif Mohammed, Vishnu K P, Laxman Das, Aniket L Chavan, Sanjay Kapoor, Nitin Burman, Bhal Singh, Dr. Gurpreet Kaur, who supported and motivated me throughout my experiments.

I would like to thank all of my friends for making these five years at IISER Mohali wonderful. Special thanks to Fidha Nazreen K M, Sandra Sajan, Lipika Taneja, Akshay P Menon, for their criticism and perspective throughout this project.

I am deeply indebted to IISER Mohali and INSPIRE fellowship for giving me the incredible opportunity to complete five years of graduate and undergraduate studies.

Finally, I would like to express my gratitude to my parents for all the support and motivation that made me accomplish whatever I am today.

List of Figures

List of Tables

Notations

FPI	Fabry Perot Interferometer
mm	millimetres
PDMS	Polydimethylsiloxane
PSF	Point Spread Function

Contents

Abstract

With the developments in the field of photonics, optical imaging plays an important role in biological studies. A few optical techniques that act as the primary steps in cellular level imaging are studied and implemented.

Light field image processing allows 3D reconstruction of objects unlike conventional imaging systems [Wu 17]. This opens up the possibility of visualizing biological structures in 3D in real-time. Something that is usually achieved using tomography. A light field imaging system for the 3D estimation of a point beam was constructed.

Ultrasound and photoacoustic imaging are non-invasive methods commonly used in medical diagnostics. The former method involves the emission of ultrasound waves and their detection after being scattered by the subject. Whereas the latter uses systems that emit light but detect ultrasound waves that are produced by the subject as a result of optical energy absorption [Xia 14]. Both techniques require the detection of ultrasound waves. Material based (piezoelectric) detectors are commonly used in diagnostics. But they are much less sensitive and have lower frequency bandwidths compared to optical detectors. Photoacoustic imaging of very small objects (in the range of 100 microns) require sensors with a frequency response ranging from a few MHz to well above 100 MHz [Wissmeyer 18]. Such wide bandwidths are possible only using optical methods. In addition, the size of a material based sensor cannot be reduced beyond a certain point as the sensitivity is very dependent on the surface area. An optical method for ultrasound detection, namely using a Fabry Perot interferometer, was studied and implemented.

Chapter 1

3D reconstruction of a laser beam using light fields

1.1 Introduction

Normally, for the construction of a 3D image, we are required to capture multiple 2D images from different perspectives as a lot of information cannot be obtained from a single image [Pollefeys 04]. But this setup can be modified by inserting a microlens array between the object and sensor, allowing one to capture light fields instead of pixel information. By doing so, angular information of light rays can be recorded, making it possible to generate multiple images of different focal depth (known as focal stacks) from a single image. These images can be used to reconstruct a 3D image. The first use of lens arrays in its primitive form was done by Lippman in his invention of integral photography [Lippmann 11]. A century later, light field was captured using a regular camera by placing a microlens array behind the lens [Ng 05]. In this camera, which is commercially available, the focus of the images can be altered post-capture and a slight parallax view is possible. By placing a microlens array in the image plane of a microscope, the light field imaging technique was extrapolated to microscopy [Levoy 06]. This allowed real-time imaging of smaller biological subjects which was not possible with the existing 3D reconstruction techniques. This was used to study neuronal activities live in tiny organisms like zebra fish [Prevedel 14].

Observing the shape of the laser beam used is very important, as many optics experiments and other applications like information transfer might require the use of lasers with specific profiles (for instance, a Gaussian profile). It is also possible that the beam shape might change over time. Normally, 2D measurement of beam width is done to profile the laser but 3D estimation could give a much more accurate picture especially in terms of change in shape with the distance covered. The technique followed by light field cameras and microscopes were used to make a 3D reconstruction of a laser beam exiting an optical fibre tip. If the reconstruction is made possible in a regular lab environment for a point beam, it can be extrapolated to more complex subjects on the cellular scale.

1.2 Light fields

Light field is radiance represented as a 4-dimensional function of position and direction in space [Levoy 06]. Any light ray in 3D space can be described using three coordinates for position and two for angles. But assuming there is no obstacle in the 3D space, the radiance along a ray remains unchanged. Thus, one dimension can be reduced, giving us a four-dimensional light field function. The 4D light field function can be parametrized in multiple ways. One way of representation is using four coordinates, u, v, s, and t, to represent the two endpoints in two parallel planes (figure 1.1 d) [Levoy 06].

In a regular imaging system, the light rays coming from one point at different angles are all recorded on the same point in the sensor (figure 1.1 a). But if a microlens array is placed after the converging lens, these angular rays passing through it will fall on different positions on the sensor and are thus recorded separately (figure 1.1 b).

Each microlens records a particular view of the object. The image produced has sub-images, each capturing a portion of the object in the frame and each pixel within a sub-image recording a specific point of view. Selecting those pixels that capture a particular perspective from each sub-image and adding them will give a complete

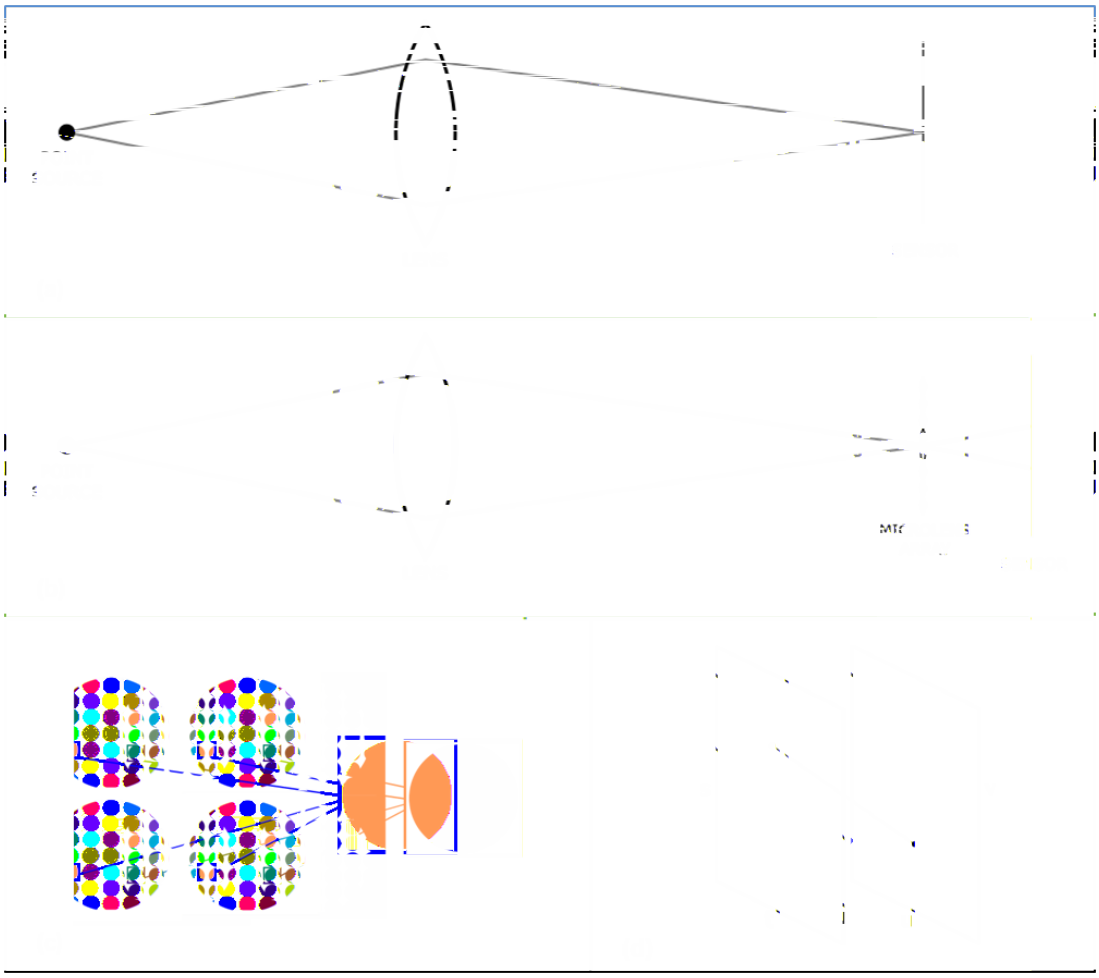

Figure 1.1: (a) Simplified ray diagram of a normal imaging system. (b) Ray diagram of an imaging system with a microlens array [Ng 05]. (c) Specific pixels from each microlens taken to form a complete image. (d) 4D light field representation.

image of the object in that perspective (in a specific focal depth) [Chiou 15] (figure 1.1 c). This can be done for each perspective thus giving images of the same object with different focal depths. This process called focal stacking is done in the *LFDisplay* software which is mentioned later.

1.3 Point spread function and 3D deconvolution

Point Spread Function (PSF) of an imaging system describes how a point source is recorded by that system. The light from a point source as it passes through the imaging system undergoes defocus and is blurred when it falls on the image sensor. It is not recorded as a single point as expected (due to diffraction and imperfections

in the lenses) [Rossmann 69]. The PSF of a point in 3D space integrated across the focal depths will be a double cone shape [Levoy 06]. The focal stack mentioned earlier is a convolution of the object by the 3D PSF. In each image of the stack, there will be portions that are blurred compared to the rest as these constitute the wider parts of the PSF cones of the respective points. In other words, the blurring is because of the PSF convoluting the image. Deconvolution can be applied on these portions by inverse filtering (i.e. multiplying the inverse of PSF with the image matrix in the Fourier domain). The deconvolved images are used for 3D reconstruction of the object. All these processes (including deconvolution and 3D reconstruction) are not explicitly done and happen in the background within the *LFDisplay* software.

1.4 Image capture of a point beam

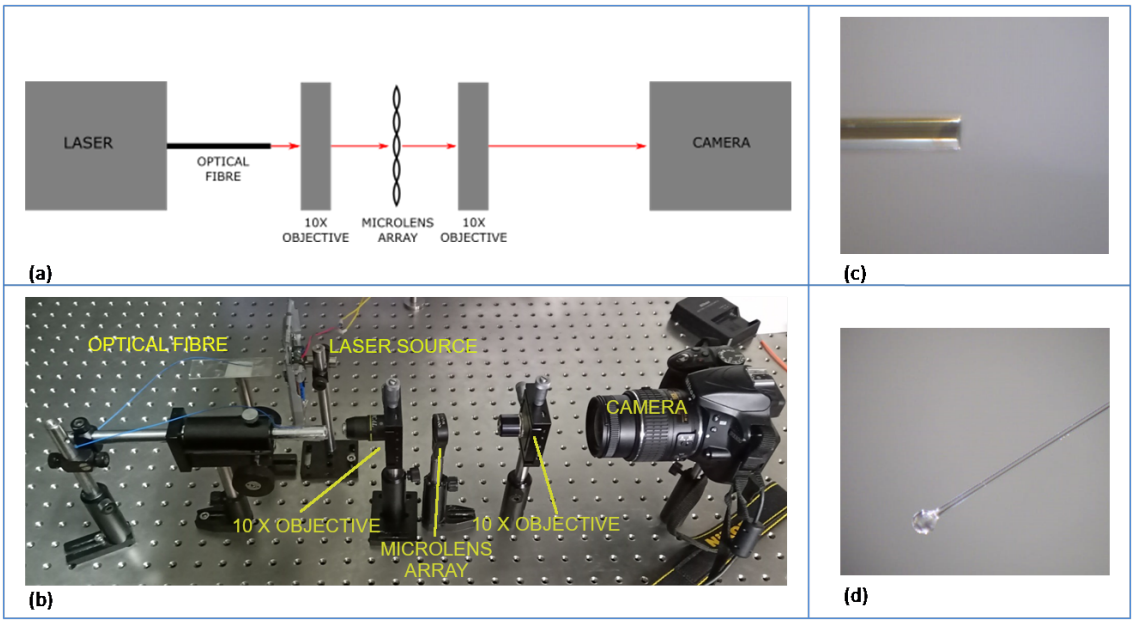

Figure 1.2: (a) Schematic diagram of the setup. (b) Experimental setup. (c) Perpendicularly cut optical fibre. (d) Optical fibre spliced to form a sphere.

A red laser obtained from a CD player was used as the source. It was coupled with an optical fibre so that light will exit the other end and act as a point beam. The cladding of the optical fibre was removed at the tips and they were perpendicularly cut using a cleaver at both ends (figure 1.2 c). One of the ends was spliced to form a spherical shape using *Fujikura* fusion splicer (figure 1.2 d). In this machine, the fibre

was placed with the tip near the electrodes. It was heated to a very high temperature by the electrodes, creating an electric arc, causing it to melt and form a spherical shape [Fan 06]. This spherical shape will act as a convex lens to diverge the light.

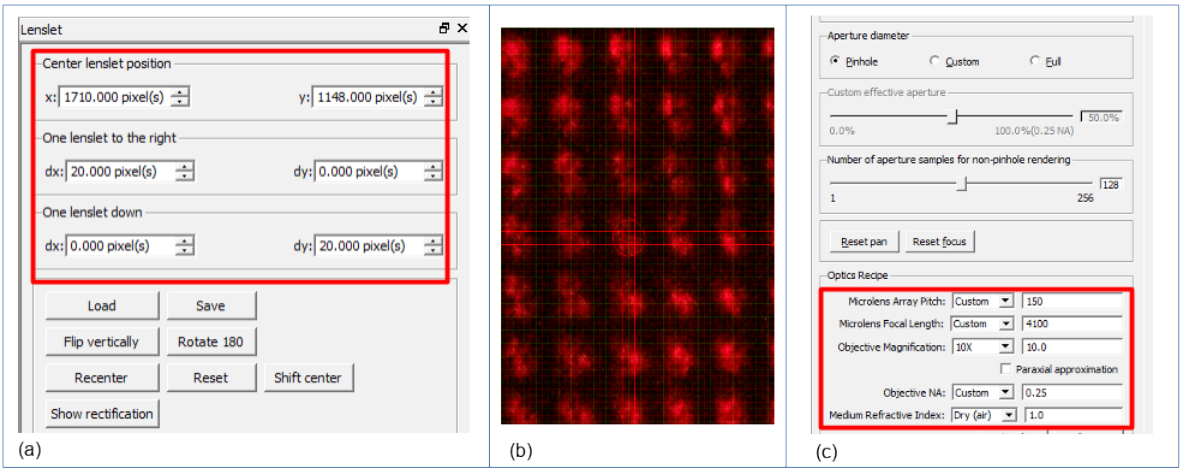

Figure 1.3: (a) Microlens position adjustment. (b) Lenslet position marker. (c) Optical characteristics.

In the setup, the optical fibre was followed by a 10x objective lens, the microlens array (*MLA 150-5C-M* from *Thor Labs*) and then another 10X lens for magnification. The final images were recorded using a *Nikon D3400* DSLR camera. The images were post-processed in *LFDisplay*. The lenslet position was specified and adjustments were made in reference to the captured image (figure 1.3 b). Other data about the optical environment and information about the lenses such as the lenslet pitch (which is the width of each microlens in the array) were also input (figure 1.3 c). A 3D estimate of the laser beam was produced by the software.

Optics data (given according to the data provided in the literature of the equipment):

- Lenslet pitch = 150 μ
- Microlens focal length = 4.1 mm
- Numerical aperture of the objective = 0.25
- Medium refractive index = 1 (air)

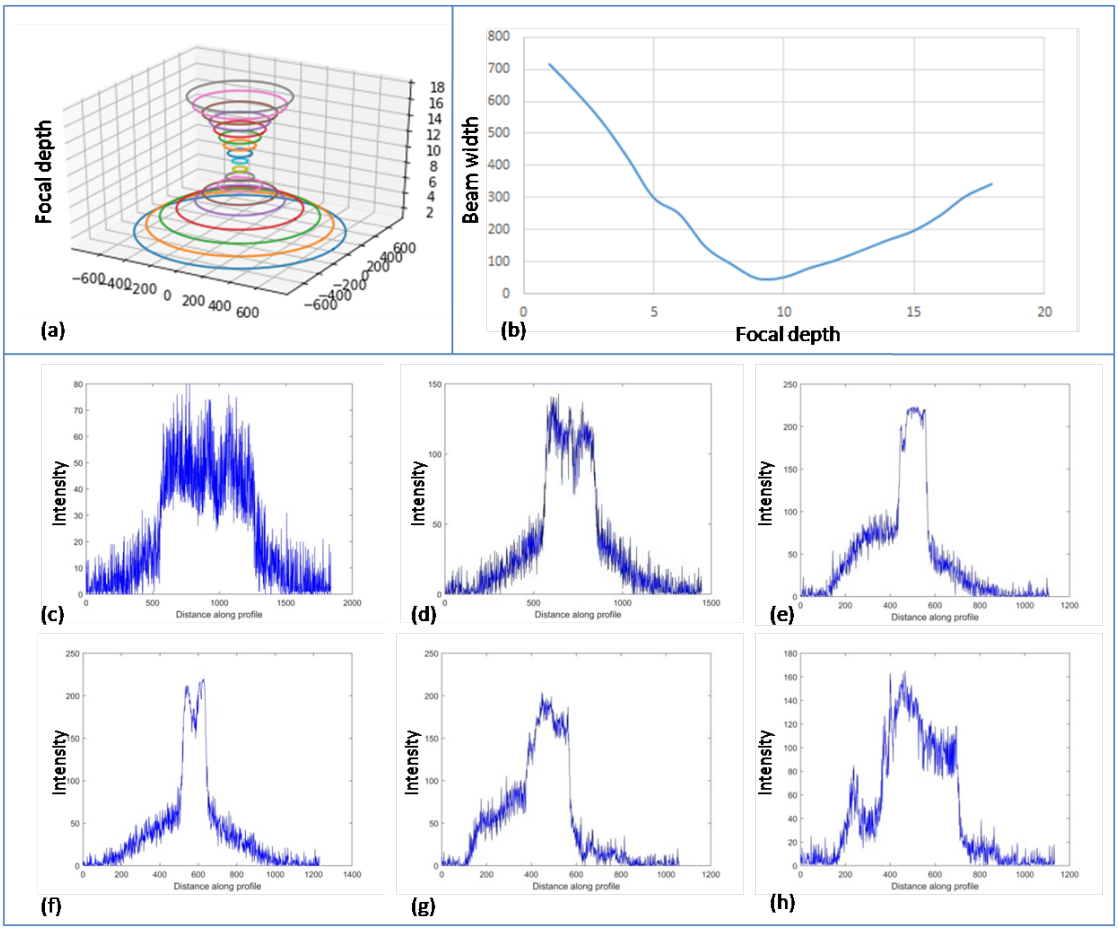

Figure 1.4: (a) 3D plot of beam width (represented by the diameter of circles) at different focal distance. (b) 2D graph of focal distance and width of the beam. (c - h) Focal depth vs intensity graphs obtained by measuring intensity across an axis.

1.5 PSF estimation in MATLAB

The laser source was coupled with the optical fibre followed by a 10x objective lens. The microlens array and the second objective were removed. The camera was focused on the beam. Several photographs were captured with different focus settings. The obtained images show the laser source roughly circular with varying sizes. The size was smallest when the optical fibre tip was in focus and it increased when the distance was changed either ways. The *'improfile'* function from the *Image Processing Toolbox* in *MATLAB* allowed drawing a line approximately through the diameter of the circle. Then the intensity of the laser beam across the line was calculated by the function [Mat 19]. This information was used to estimate the beam width of the source at different focal depths. The double cone structure of PSF was attained when a 3D graph between focal depth and beam width was plotted. As only a few points across

the focal axis were chosen for measurements, it is not an accurate calculation but rather an approximation of the shape.

1.6 Results

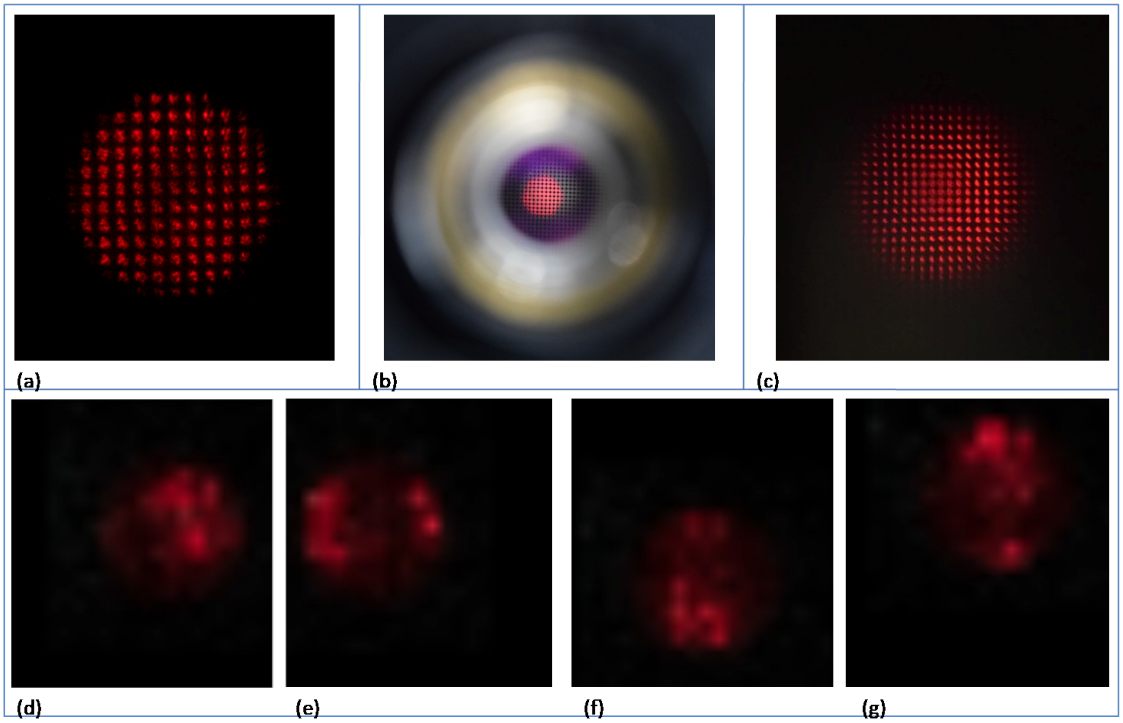

Figure 1.5: (a) Image of point beam captured through the microlens array followed by a 10x objective lens. (b) Similar image captured at brighter lighting conditions. (c) Image captured without the second objective lens. (d - g) Different shots of 3D reconstruction of the point beam produced in *LFDisplay*.

An image of the point beam consisted of circular sub-images from each lenslet (figure 1.5 a). Each microlens recorded a specific portion of the subject and each pixel within a microlens captured a particular point of view of that portion. Adding the corresponding pixels from each microlens gives the complete image of the subject in that point of view. This focal stack produced from a single photographic capture was used by *LFDisplay* to reconstruct a 3D shape (figure 1.5 d-g). It was possible to tilt the reconstructed beam at any direction up to a limit (Set by the aperture of the lens. Aperture defines the maximum angle from which light fields can enter). The reconstructed beam was of very low resolution because a microlens image which was used for the construction records angular information with a trade-off in spatial

resolution [Levoy 06].

1.7 Future Plans

While recording detailed angular information, spatial resolution is greatly sacrificed. Due to this, the reconstructed shape is blurred and inaccurate. The quality of the construction can be improved only by increasing the information collected by the initial photograph. This can be achieved by adjusting the environment and setup condition such that the number of microlenses that gather the information of the subject is increased. When the 3D shape of a point beam can be accurately reconstructed, it can be extrapolated to light coming from further complex structures in the cellular level.

Chapter 2

Detection of ultrasound using flexible Fabry Perot interferometer

2.1 Introduction

Ultrasound imaging is a very useful diagnostic method because it is non-invasive and relatively harmless. It does not use ionizing radiation or toxic chemicals for the detection process. Commercially, piezoelectric transducers are used for ultrasound detection. But they are very bulky, have a limited frequency bandwidth, and interfere with other optical imaging processes (as they are opaque) [Dong 16]. Optical methods can be applied instead, to tackle these limitations. One of the options is to incorporate a Fabry Perot interferometer in the detector.

A Fabry Perot interferometer (FPI) is an optical device consisting of two parallel mirrors with high reflectivity on the inner surfaces. This instrument was developed by Charles Fabry and Alfred Perot in 1899 [Vaughan 89]. The light beams formed due to multiple reflections between the mirrors act like different sources and interfere, forming a fringe pattern. The pattern is determined by the wavelength of light and the distance between the mirrors. A change in distance between the reflective surfaces cause a shift in the fringe pattern. These characters allow its wide range of applications in spectroscopy and precise measurements of light.

Fabry Perot based sensors have found applications in various fields like medicine and spectroscopy. An FPI constructed on a single-mode optical fibre is used as an invasive pressure measurement device in medical diagnostics for the monitoring of arterial blood pressure, intracranial blood pressure, etc. [Wang 05]. Similar setup is also used to detect the pressure exerted by the ultrasound waves, as it causes a variation in the refractive index of the cavity [Alcoz 90]. In the following experiment, one of the reflective surfaces in a macroscopic FPI setup is modified so that it can detect sound waves.

2.2 Modifying a Fabry Perot interferometer

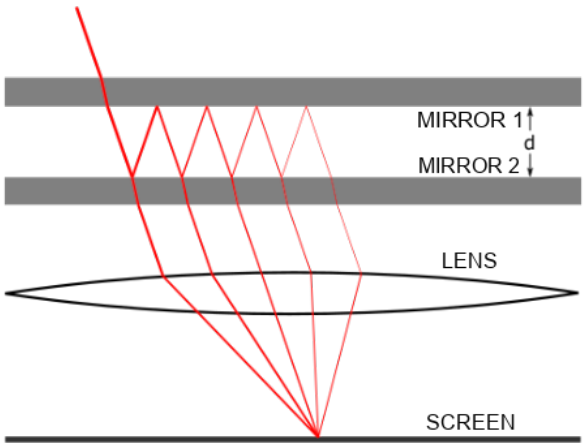

Figure 2.1: Path of the laser in an FPI.

Each time a light beam hits a mirror it is partially reflected and refracted. Thus, the reflected light will have a lower intensity compared to the original light. The light beam that enters the space between the mirrors in an FPI gets reflected multiple times until the intensity becomes negligibly small (figure 2.1). All the beams that leave the parallel mirror chamber are converged on a screen to interfere. Since each light wave traverse different path and undergo different number of reflections, there will be relative phase difference when they interfere. If two interfering light waves are in phase (i.e. they have similar peaks), the peaks add up and the interference is constructive. If the peaks are opposite, they will subtract and the interference will be destructive. In other words, if the path difference of two waves is an integral multiple of the wavelength, the intensity will be maximum. The path difference,

$$2dcos\beta = m\lambda$$

where β is the incident angle of the light ray, d the distance between the mirrors and λ the wavelength of light. The interference pattern formed will be circular (since the beams are converged on a screen) with consecutive dark and light bands. When the reflectivity is high, the bright rings produced will be sharp. The number of reflections are also proportional to the sharpness of the rings.

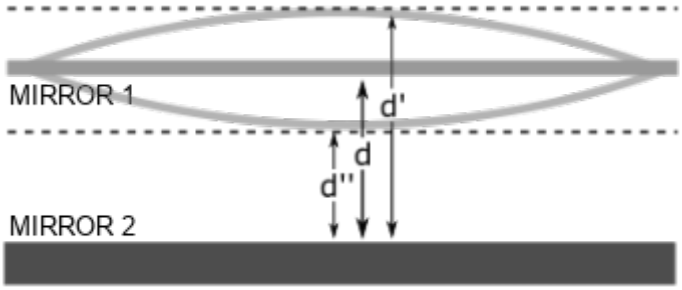

Figure 2.2: Flexible mirror.

When the distance between the mirrors is changed, the path difference of light waves is changed thus altering the interference pattern with either formation of new fringes or collapse of existing ones. This property can be utilized to detect sound waves by modifying the setup. A flexible material which can vibrate when exposed to sound waves can be used as the top mirror (figure 2.2). These vibrations change the distance between the lenses in an oscillatory fashion, in turn causing an oscillatory movement in the fringes. This can be used to detect the presence of sound waves and can further be extrapolated to ultrasound waves. Studying the extent of change within the interference patterns due to a sound of known frequency can be used to calibrate the setup. Then the frequency of an unknown sound can be calculated from the changes in the fringes.

2.3 Designing a flexible mirror

The flexible mirror required for the modified FPI is constructed using a silicon-based organic polymer called *Polydimethylsiloxane* (PDMS). PDMS acts like a viscous fluid at room temperature. It can be poured in a mould with a curing agent added so that

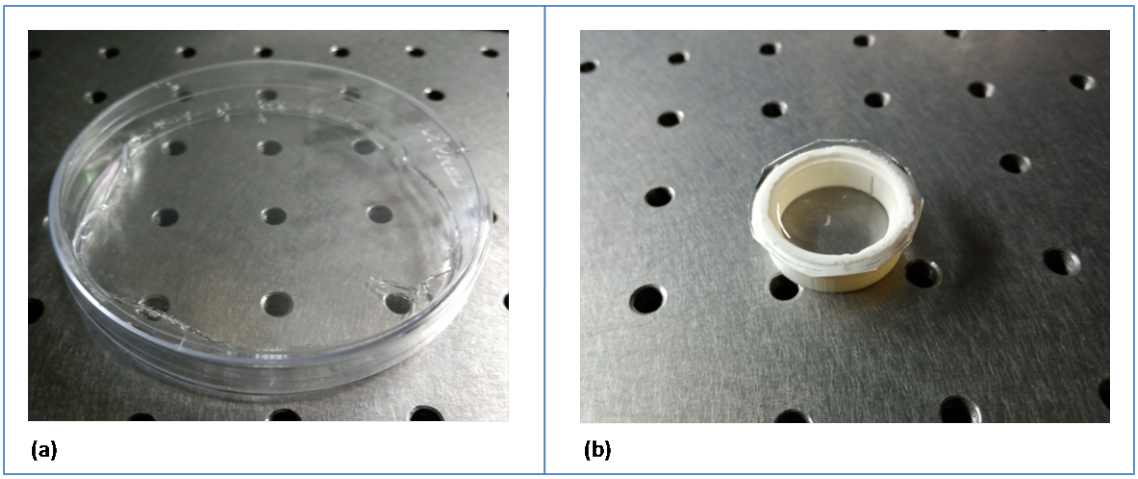

Figure 2.3: (a) PDMS sheet cured in a petri dish. (b) PDMS film attached on the mount.

it hardens to solid and takes the shape of the mould. Its transparency allows it to be used in optics experiments. It can be used to make custom prisms, lenses and reflecting surfaces. It is easy to design compared to glass and construction can be done in the lab. Moreover, it is not rigid like glass and can be made flexible if cured as a thin sheet. So, it was used to construct thin and flexible reflecting surfaces for the modified interferometer.

Sylgard 184 from *Dow Corning*, a commercially available PDMS kit, was used for the purpose. It constitutes a base part and a curing agent which have to be mixed at 10:1 ratio. For the preparation of PDMS samples, 2 grams of base and 0.2 grams of curing agent were used. The mixture was poured in a petri dish and mixed thoroughly for around 2 minutes. The 3D printed mount on which the flexible lens is to be mounted was dipped in the mixture. This was done so that the substance sticks on the mount when it cures (figure 2.3 b). The attempt to stick the sheet on the mount after it cured failed as the PDMS layer stuck on to the surface of the petri dish and tore when tried to remove (figure 2.3 a). The mixture was left at room temperature to be cured for about 24 hours.

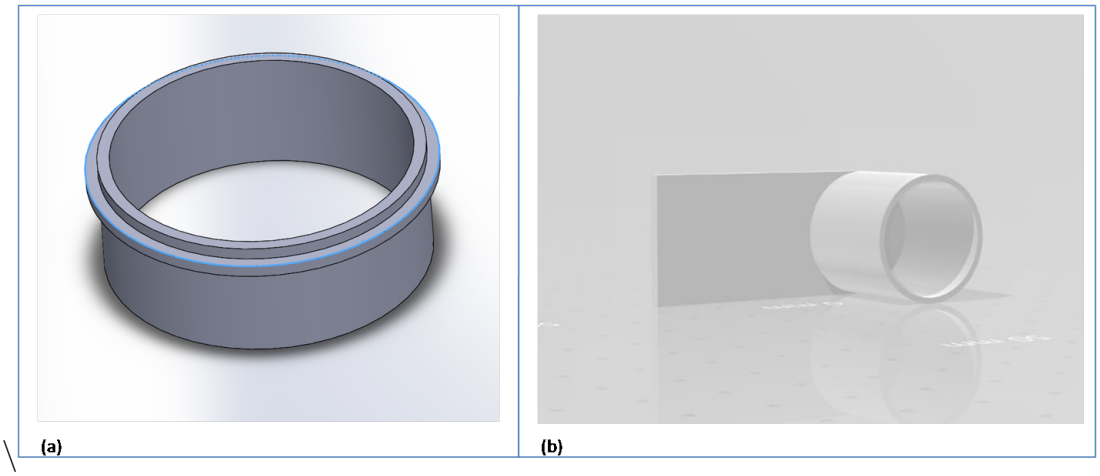

Figure 2.4: (a) mount for the flexible mirror. (b) Mount for the second mirror.

2.4 3D printed mounts

The mounts for the lenses were designed in the 3D design program called *SolidWorks*. The models were prepared for printing using the *Ultimaker Cura* software and printed in the *Ultimaker 2+* 3D printer. The mount for the top lens is a hollow cylinder with an inner diameter of 24 mm and an outer diameter of 26 mm. There is a protruding part with a diameter of 28 mm (figure 2.4a) which helps in holding the mount. The mount for the second lens has a hollow cylindrical structure with a rectangular extension which helps to connect it to a stand such that it does not hinder the movement of the mount. The cylindrical part has a height of 22 mm, an inner diameter of 19 mm and an outer diameter of 21 mm. This is so that the glass slide used as the second reflecting surface, with 20 mm diameter, can be placed on it easily. The rectangular part is 50 mm in length from one end to the other (including the cylinder) and 2 mm in height. The second mount has an outer diameter less than the inner diameter of the first mount so that they can overlap. This is required as the distance between the lenses have to be within a range of few microns.

2.5 Sputtering a reflective coating

While circular PDMS sheets were used as the flexible first mirror, thin circular glass slides of 20 mm diameter were used as the non flexible second reflective surface. These surfaces were coated with reflective film of gold using a sputtering machine.

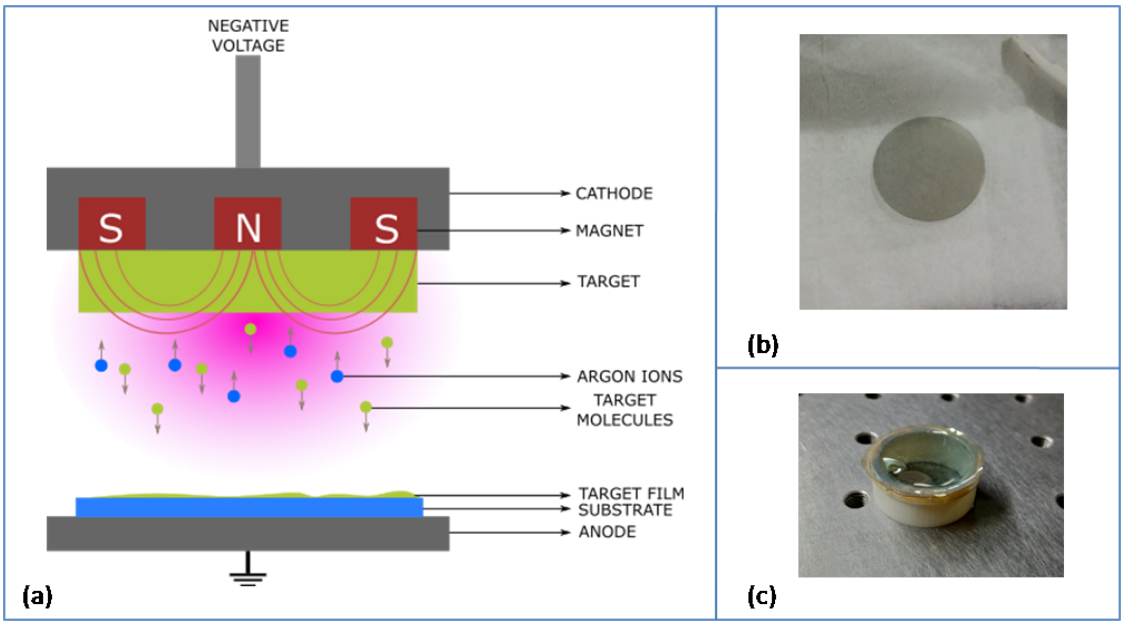

Figure 2.5: (a) working of a sputtering machine. (b) gold-coated glass slide. (c) gold-coated PDMS film.

2.5.1 Working of a sputtering machine

Air is continuously pumped out from the sputtering chamber to create a near vacuum condition and then argon is continuously pumped in. A heavy negative potential is applied to the target material (here gold) which ionizes the argon gas and leads to the formation of plasma. An inert gas is used so that no chemical reactions happen with the target material. The plasma consists of argon atoms, argon ions and free electrons. A magnet below the target makes sure that the plasma surrounds it. The free electrons further collide with the argon atoms and ionize them. The positively charged argon ions bombard with the target as it is in a highly negative potential. This causes some of the target molecules to be sprayed with high kinetic energy in the opposite direction thus hitting the substrate (here PDMS sheet or glass slide).

2.5.2 Reflectivity

The reflectivity is determined by the extend of coating. For instance, if a substrate is heavily coated, the reflectivity will be very high and the intensity of light passing through will be very low. Controlling the thickness was not possible in the sputtering machine used in the lab. So, it had to be adjusted loosely by managing the sputtering

time. The thickness does not have to be very accurate as the relative reflectivity of the two surfaces is more important. The first mirror was coated for about 50 seconds while the second mirror was coated for about 90 seconds. The first mirror was coated to have relatively lower reflectivity so that most of the light enters the cavity while the second mirror was coated for higher reflectivity so that light rays are reflected in the space multiple times for a longer period.

2.6 Experimental Setup

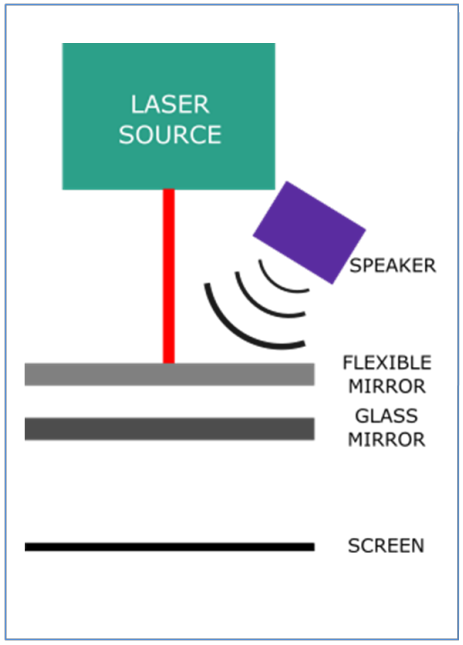

Figure 2.6: Schematic diagram of the setup.

The experiment was set up on an optical table with vibration isolators that float the table using compressed air. This isolates the setup from any surrounding vibrations coming through the floor.

A red laser obtained from a CD player was used as the source in the experiment. It was placed vertically above the first mirror at a distance of about 3 centimetres using a stand. The light converged within the range of the first reflecting surface. The 3D printed mounts holding the mirrors were connected to stands having single-axis translators. So the distance between the mirrors can be changed in a very small magnitude. This is important as it was later observed that a small change in the

distance could cause a drastic change in the fringe patterns. Both the mirrors are held horizontally with the second mirror directly below the first. A white screen was placed on the table which was at a distance of about 20 centimetres below the second reflecting surface. So the light beams coming from the surface can converge and interfere at the screen to form a fringe pattern.

2.7 Results

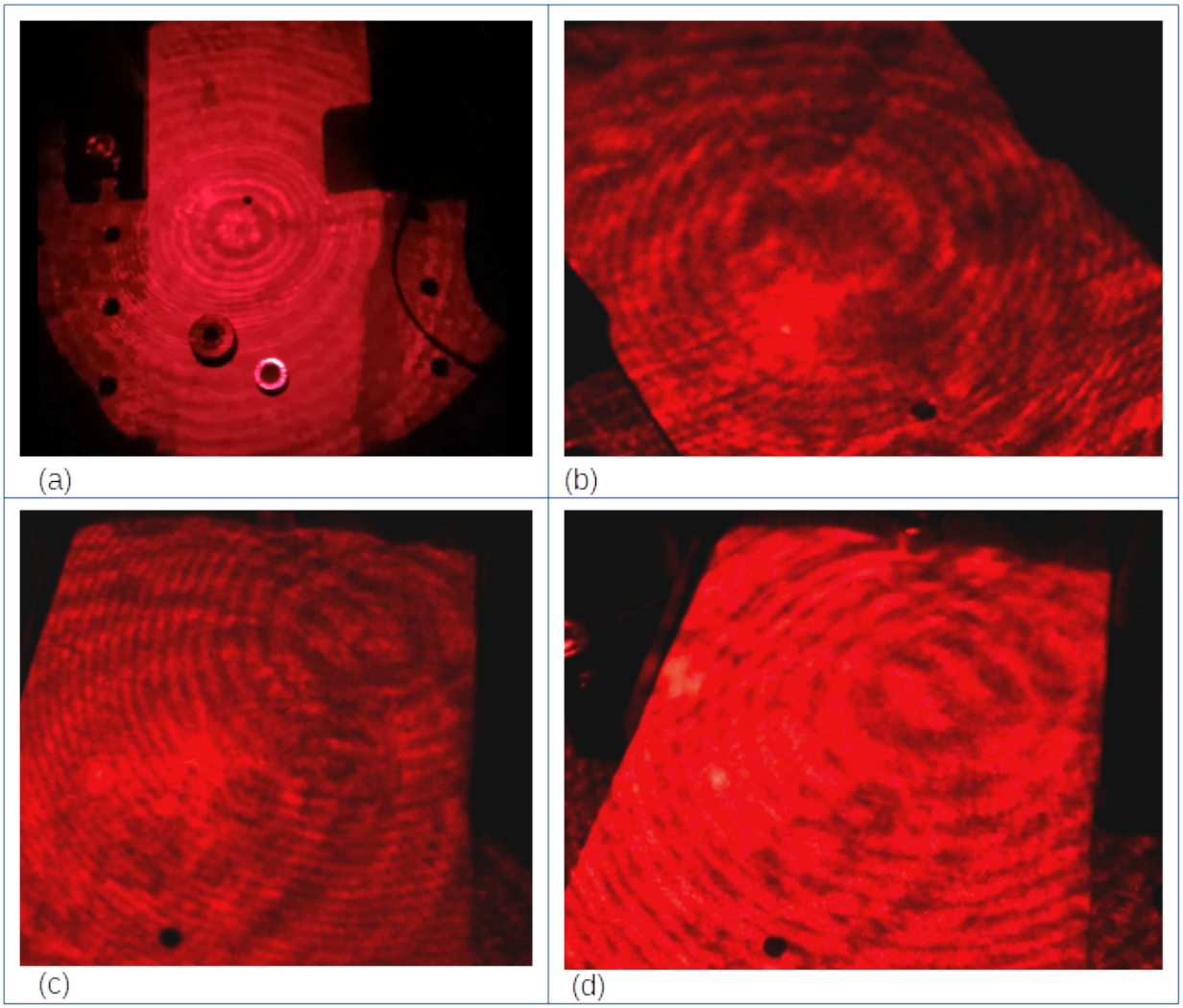

Figure 2.7: Interference fringe patterns

The distance between the mirrors was adjusted to produce fringes. It was found that mirrors have to be very close (within a range of few microns) for the fringes to appear. An increase in the distance between the mirrors could reduce the number of

reflections drastically. This reduces the number of beams interfering thus decreasing the contrast of fringe patterns. Besides, tiny dust particles and imperfections on the coated surfaces resulted in blotches on the image formed on the screen. The scratches present on the laser source also added to this irregularity.

It was found that either new fringes formed or older ones collapsed when the distance between the mirrors was changed even slightly. The change was drastic compared to the distance covered. The translators were used so that this movement was controlled without much difficulty.

A speaker producing a short high pitched sound (within the audible range) in regular intervals was placed slightly above the laser source. The fringes were found to fluctuate slightly at the instant this sound was produced and go back to normal when it stopped. This implies that the sound causes vibrations on the flexible mirror changing the distance between the mirrors and in turn, causing fluctuations in the fringe pattern.

Sound with a frequency above audible range produced using the same speakers did not cause any change in the fringe patterns. As the frequency of the sound increased the change in the fringes became negligible or even unnoticeable. This could be because of the inability of a normal speaker to produce sounds of frequency above the audible range in considerable intensity.

2.8 Future Plans

Unfortunately, extending the experiment to the ultrasound range was not possible due to the Covid 19 situation.

The disturbances in the fringe pattern have to be quantified. The extent of change in the fringes during the oscillation has to be recorded. This can be related to the frequency of the sound produced. The relation between frequency and fringe change can be plotted and then calibrated. This graph can be extrapolated to find the frequency of an unknown sound from the change in the fringe pattern.

It was observed that higher frequency sounds produced using normal speakers did not give any results. The production of ultrasound waves has to be done using a

transducer instead, so that waves of significant energy are emitted. This also allows the placement of the source closer to the mirror as it is much smaller compared to a speaker. This will increase the chance of larger vibrations on the flexible surface.

Bibliography

[Alcoz 90] Jorge J Alcoz, CE Lee & Henry F Taylor. *Embedded fiber-optic Fabry-Perot ultrasound sensor*. IEEE transactions on ultrasonics, ferroelectrics, and frequency control, vol. 37, no. 4, pages 302–306, 1990.

[Chiou 15] Pei-Chuen Chiou & Jia-Han Li. *Effects of number of Lenses in microlens arrays on field of view in integral imaging systems*. International Journal of Automation and Smart Technology, vol. 5, no. 2, pages 107–111, 2015.

[Dong 16] Biqin Dong, Cheng Sun & Hao F Zhang. *Optical detection of ultrasound in photoacoustic imaging*. IEEE Transactions on Biomedical Engineering, vol. 64, no. 1, pages 4–15, 2016.

[Fan 06] Kuang-Chao Fan, Hung-Yao Hsu, Po-Yuan Hung & Weili Wang. *Experimental study of fabricating a microball tip on an optical fibre*. Journal of Optics A: Pure and Applied Optics, vol. 8, no. 9, page 782, 2006.

[Levoy 06] Marc Levoy, Ren Ng, Andrew Adams, Matthew Footer & Mark Horowitz. *Light field microscopy*. In ACM SIGGRAPH 2006 Papers, pages 924–934. 2006.

[Lippmann 11] G Lippmann. *Integral Photography a new discovery by Professor Lippmann*. Scientific American, August, vol. 19, page 191, 1911.

[Mat 19] The Mathworks, Inc., Natick, Massachusetts. *MATLAB version 9.6.0.1072779 (R2019a)*, 2019.

[Ng 05] Ren Ng, Marc Levoy, Mathieu Brédif, Gene Duval, Mark Horowitz, Pat Hanrahan*et al. Light field photography with a hand-held plenoptic camera*. Computer Science Technical Report CSTR, vol. 2, no. 11, pages 1–11, 2005.

[Pollefeys 04] Marc Pollefeys, Luc Van Gool, Maarten Vergauwen, Frank Verbiest, Kurt Cornelis, Jan Tops & Reinhard Koch. *Visual modeling with a hand-held camera*. International Journal of Computer Vision, vol. 59, no. 3, pages 207–232, 2004.

[Prevedel 14] Robert Prevedel, Young-Gyu Yoon, Maximilian Hoffmann, Nikita Pak, Gordon Wetzstein, Saul Kato, Tina Schrödel, Ramesh Raskar, Manuel Zimmer, Edward S Boyden*et al. Simultaneous whole-animal 3D imaging of neuronal activity using light-field microscopy*. Nature methods, vol. 11, no. 7, pages 727–730, 2014.

[Rossmann 69] Kurt Rossmann. *Point spread-function, line spread-function, and modulation transfer function: tools for the study of imaging systems*. Radiology, vol. 93, no. 2, pages 257–272, 1969.

[Vaughan 89] M Vaughan. The fabry-perot interferometer: history, theory, practice and applications. CRC press, 1989.

[Wang 05] Xingwei Wang, Juncheng Xu, Yizheng Zhu, Bing Yu, Ming Han, Kristie L Cooper, Gary R Pickrell & Anbo Wang. *An optical fiber tip pressure sensor for medical applications*. In Quantum Electronics and Laser Science Conference, page JTuC46. Optical Society of America, 2005.

[Wissmeyer 18] Georg Wissmeyer, Miguel A Pleitez, Amir Rosenthal & Vasilis Ntziachristos. *Looking at sound: optoacoustics with all-optical ultrasound detection*. Light: Science & Applications, vol. 7, no. 1, pages 1–16, 2018.

[Wu 17] Gaochang Wu, Belen Masia, Adrián Jarabo, Yuchen Zhang, Liangyong Wang, Qionghai Dai, Tianyou Chai & Yebin Liu. *Light Field*

Image Processing: An Overview. IEEE Journal of Selected Topics in Signal Processing, vol. PP, pages 1–1, 08 2017.

[Xia 14] Jun Xia, Junjie Yao & Lihong V Wang. *Photoacoustic tomography: principles and advances*. Electromagnetic waves (Cambridge, Mass.), vol. 147, page 1, 2014.